Electronic Journal of Structural Engineering

Original Article

Cite this: DOI:10.56748/ejse.24797

Received Date: 15 March 2025
Accepted Date:22 September 2025

1443-9255
https://ejsei.com/ejse

Investigation of Plant Fiber-Reinforced Cementitious Composites for Permanent Formwork in Foundation Beams

Xinyuan Wang [a], Ping Li [a*], Xuansheng Cheng [a], Mei Lin [a], Shunli Ma [b], Xufeng Du [a]

[a] School of Civil and Hydraulic Engineering, Lanzhou University of Technology, Lanzhou 730050, China
[b] Henan Key Laboratory of Green Building Materials Manufacturing and Intelligent Equipment, Luoyang 471023, China
*Corresponding author: lzlqliping@126.com

Abstract

This paper aims to solve the problems of extensive labor input and long construction periods of traditional foundation beam brick formwork. To this end, plant fiber-reinforced cementitious composites (PFRCC) panels were proposed to replace conventional foundation beam brick formwork. Tests and finite element analyses were conducted on the PFRCC panels used as permanent formwork for foundation beams, based on a construction project in Lanzhou City, Gansu Province, China. The results indicate that the maximum bending stress of the PFRCC panels utilized as permanent formwork for foundation beams is 0.4069 MPa, occurring at the junction between the side and bottom forms, which is significantly lower than the specified design strength of 13.7 MPa. Furthermore, the maximum deformation recorded was 1.528 mm at the mid-span of the side formwork, remaining below the permissible limit of 2.5 mm. The bending strength and stiffness deformation meet the design requirements, which shows that the PFRCC panels can be used as the permanent formwork of the foundation beam.

Keywords

PFRCC, Foundation beam, Permanent formwork, Three-point bending test, Green building

1. Introduction

With the continuous progress and rapid development of urban construction and industrialization, the energy consumption of buildings will increase year by year and occupy the dominant position of energy consumption for a long time. Therefore, building energy conservation needs to be improved. At present, we focus on promoting green prefabricated new building forms. In the past, foundation engineering mainly adopted traditional brick formwork construction technology. However, there are some problems, such as extensive labor input, high labor cost, prolonged plastering intervals, and other wet operation technology. PFRCC panels have good machinability, high strength, toughness, impermeability, and frost resistance. Therefore, this paper proposes using PFRCC panels instead of the traditional foundation beam brick formwork.

Currently, many kinds of fibers are applied in practical projects such as walls, beams and columns. (Leblouba et al., 2022; Li et al., 2023; Wang et al., 2025). Adding fiber to cement can effectively delay and prevent micro-crack development and improve cement performance. (Tiberti, 2018; Conforti et al., 2019; Empelmann et al., 2020; Oettel., 2022 and Oettel et al., 2023). Single fiber pull-out and fiber-matrix interface interaction play an important role in understanding the mechanical behavior of fiber-reinforced cementitious composites. Hemmatian et al. (2023) proposed a calculation model for predicting the maximum pull-out force and corresponding bond-slip of fibers through a large number of experiments and literature investigations. Haido. (2020) introduced a new basalt fiber reinforced concrete (BFRC) constitutive model to provide a comprehensive solution for the finite element method to study the performance of BFRC beams under bending. In addition to various fibers, the possibility of using multiple plastic waste to manufacture high-performance concrete has also become a research subject in recent years. (Väntsi et al., 2014; Keskisaari et al., 2016; Turku et al., 2017).

Formwork engineering is a general term for a series of technical work and completed entities such as the design, installation, and demolition of concrete pouring formwork and its supports. Based on the materials used, formwork can be categorized into various types, including wood, steel, plywood, plastic, aluminum alloy, and concrete, among others. Although formwork plays a vital role in building engineering, it has yet to benefit from the rapid development of structural engineering. Most of the studies are in conventional forms, such as wood and steel formwork, which can be proven in the literature (Arslan et al., 2005; Puente et al., 2010; Prosk et al., 2014; Zhang et al., 2016). Scholars first proposed using fiber-reinforced polymer (FRP) materials to enhance permanent formwork in 1998. (Hall and Mottram, 1998). Li et al. (2015) solved the problem of brittle cracking of dam concrete materials due to temperature gradient during mass construction and operation by using nano-modified ultra-high toughness cement-based composite permanent formwork for thermal insulation and anti-seepage. Meng et al. (2016) proposed using ultrahigh-performance concrete (UHPC) panels reinforced with glass fiber-reinforced polymer (GFRP) grids as permanent formwork. They found that it has the advantages of rapid construction, improved crack resistance, and prolonged structural life. Li et al. (2019) provided an alternative for developing cement fiberboard as a lightweight permanent formwork system, which can promote the thermal and acoustic comfort of green buildings. Huang et al. (2017) adopt Ultra High Toughness Cementitious Composite (UHTCC) to develop a reinforced permanent formwork, which can not only withstand the load imposed before pouring and is helpful to improve the bearing capacity of the remaining life of the structure. Kim et al. (2008) used glass fiber-reinforced concrete (GFRC) as a bridge formwork.

In summary, many scholars have tried to improve the mechanical properties of fiber-reinforced cementitious composites by adding different fibers to cement-based materials and have researched fiber-reinforced cementitious composites as permanent formwork. Still, few scholars have studied the application of PFRCC panels as permanent formwork on foundation beams. (Tian et al., 2020; Wang et al., 2021; Geng et al., 2024). In this paper, the mechanical properties of PFRCC panels were studied in detail by a three-point bending test. Based on the construction project of a community in Lanzhou City, Gansu Province, China, the field test and finite element simulation analysis were carried out to apply PFRCC panels as permanent formwork on the foundation beam.

2. Materials and Methods

2.1 Materials composition

As indicated in Table 1, the composition of the cement matrix in PFRCC includes CEM I 42.5 N cement, fly ash, quartz sand, water, and polycarboxylate superplasticizer. Standard cube samples of cement, each measuring 150 mm × 150 mm × 150 mm, were prepared, and the compressive strength of the cement matrix after 28 days is 45.8 MPa. As illustrated in Figure 1, bamboo pulp fibers were employed in the PFRCC, with an average fiber length of approximately 2.04 mm (This data is provided by the fiber manufacturer). The fibers occupied a volume fraction of 6 % in the PFRCC. Table 2 illustrates the main performance characteristics of plant fiber.

Fig. 1 Bamboo pulp fiber

Table 1. Composition of the cement matrix

CEM I 42.5 N/ (Kg/m³)	Fly ash/ (Kg/m³)	Quartz sand/ (Kg/m³)	Water/ (Kg/m³)	Superplasticizer/ (Kg/m³)	Water-binder ratio (W/B)
550	650	550	395	5.225	0.33

Table 2. Main performance parameters of bamboo fiber

Density/ (g/cm³)	Tensile strength/ (MPa)	Diameter/ (μm)	Elastic modulus/ (GPa)	Extension at break/ (%)	Length/ (mm)
1.1	350	17	22	5.8	2.04

2.2 Three-point bending test

The test setups for the three-point bending test are shown in Figure. 2. The three-point bending test on the PFRCC panels was conducted using a universal mechanical testing machine with a 100 kN capacity, where the span between the two supports at the base of the loading apparatus was configured to be 200 mm. This test was performed following the Test methods for fiber cement products (Standardization Administration of China, 2014). The specimen's dimensions were 250 mm for length, 100 mm for width, and 18 mm for thickness. Three sets of specimens were used to prevent test errors.

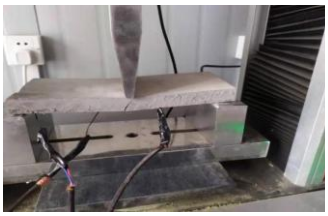

(a)Test equipment diagram

(b)Failure pattern of specimens

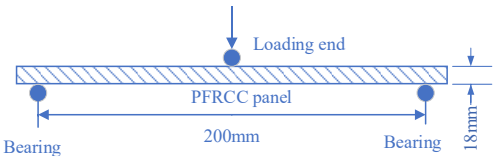

(c)Three-point bending test loading diagram

Fig. 2 Three-point bending test diagram

In this test, a static load with a loading rate of 10 mm/min was used. The panel's bending strength was computed using Equation (1), and the result was modified to 0.1 MPa.

$$\sigma_m = \frac{3P_m L}{2be^2} \quad (1)$$

where σ_m represents bending strength (MPa); P_m represents failure load (N); L represents distance between bearings (mm); b represents the width of the specimen section (mm); e represents specimen section thickness (mm).

2.3 Fiber-matrix joint constitutive relation model

Selection of constitutive relation between fiber and matrix

In this paper, the cement matrix adopts the plastic damage model of concrete. The main performance parameters of bamboo fiber are shown in Table 2, and the constitutive relation curve is shown in Fig. 3. When simulating PFRCC using finite element software, establishing the constitutive relationship curve for plant fibers is relatively straightforward. Plant fibers can be assumed to exhibit linear elastic characteristics until reaching a certain tensile strength, at which point fracture occurs. Truss elements are employed to model plant fibers.

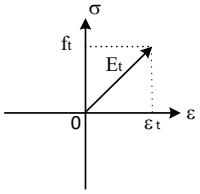

Fig. 3 Fiber constitutive relation curve

where σ represents stress (MPa); ξ represents strain; f_t represents tensile strength (MPa); ξ_t represents the strain corresponding to f_t; E_t represents elastic modulus (MPa).

Numerical simulation of single fiber pull-out

One crucial approach for investigating cement-based fiber composite materials entails analyzing the load-displacement relationship curve of a single fiber pulled out from a cement matrix. This curve serves as an indicator of the fiber's performance changes within the cement matrix. Based on the single fiber pull-out test for plant fibers in a cement matrix (Kochova et al., 2020), this study developed a fiber-matrix joint constitutive relation model through finite element numerical simulation.

In a cement matrix, the pull-out behavior of plant fibers involves three stages: the elastic interface stage, the debonding stage, and the sliding stage. However, in conventional single-fiber pull-out theory, researchers neglected the elastic stage at the interface. They assumed that the elastic elongation of the fibers was negligible compared to the slip displacement during pull-out. (Li, 1993). Therefore, the fiber is treated as a rigid body, disregarding the elastic elongation of the fiber itself and solely considering the rigid body displacement of the fiber within the cement matrix. The unbonded portion of the fiber during the debonding stage is primarily governed by the chemical bonding force, which is represented by a parameter Gd that characterizes the chemical bonding properties between the fiber and matrix. The elastic elongation of the deboned fiber takes place within the cement matrix, while the sliding friction force remains constant at an initial value of τ_0 and is uniformly distributed along the deboned fiber. The slip stage of the fiber is predominantly controlled by the sliding friction force. A friction factor β was introduced to characterize the variation in the sliding friction force during pull-out. Furthermore, it has been suggested that bending and surface roughness of fibers in the cement matrix diminish the effect of Poisson's ratio; thus, Poisson's ratio influence from the fibers was not considered. The relationship between the external load P at the pull-out end of the fiber and the displacement δ of the fiber relative to the matrix cracking surface was established, as expressed in Equation (2).

$$P = \sqrt{\frac{\pi^2 \tau_0 E_f d_f^3 (1+\eta)}{2}\delta + \frac{\pi^2 G_d E_f d_f^3}{2}} (0 \le \delta \le \delta_0) \quad (2)$$

Where E_f is fiber elastic modulus, d_f represents fiber diameter, η represents the parameter representing the ratio of effective fiber stiffness to effective matrix stiffness, δ_0 represents the maximum pull-out displacement of the fiber in the debonding stage, which can be obtained from Equation (3). L_e represents the embedding depth of plant fibers in the cement matrix.

$$\delta_0 = \frac{2\tau_0 L_e^2 (1+\eta)}{E_f d_f} + \sqrt{\frac{8 G_d L_e^2 (1+\eta)}{E_f d_f}} \quad (3)$$

In the slip stage, the behaviour of fiber is primarily governed by sliding friction. A friction factor β was introduced to characterize the variation in sliding friction force among different fibers. A negative value of β ($\beta < 0$) indicates slippage softening of the fiber within the cementitious matrix, a value of zero ($\beta = 0$) corresponds to constant friction slip, while a positive value ($\beta > 0$) signifies slip hardening behavior. Aiming at the slip-hardening phenomenon, Li proposed a linear variation model for the interfacial shear stress. It can be expressed as Equation (4).

$$\tau = \tau_0 \left(1 + \beta \frac{S}{d_f}\right) \quad (4)$$

Where $S = \delta - \delta_0$, considering that the fiber is a rigid body in the slip stage and there is only a uniform sliding friction force τ on the fiber surface. For the fiber with buried length L_e, the relationship between drawing load P and fiber drawing displacement δ can be obtained, as shown in Equation 5. Table 3 lists the parameters on the interface. (Li., 1993; Guo et al., 2022)

$$p = \pi d_f \tau_0 (1 + \beta(\delta - \delta_0)/d_f (L_e - \delta + \delta_0) \quad (5)$$

Table 3. The main mechanical parameters of the interface

Parameter	τ_0	G_d (J/m²)	β
Adopted value	1.31	1.08	0.308

In Figure. 4, to accurately simulate the comprehensive mechanical behavior of fibers in the matrix, this study considers the elastic stage in addition to the deboned stage and slip stage. Based on the simulated pull-out behavior of individual fibers, this study develops a constitutive model for the fiber-matrix interface that quantitatively describes the mechanical interactions between plant-based reinforcements and cementitious matrices.

In Figure. 5, since the plant fiber is embedded within the cement matrix and does not experience slipping relative to the matrix, the displacement X on the right surface of the cement matrix is considered as the elongation length of the fiber within the matrix, and P is the actual load on the fiber.

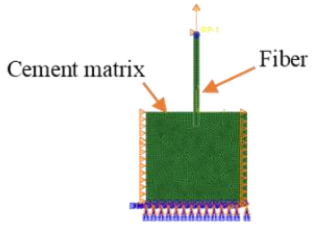

Fig. 4 Single fiber pull-out simulation diagram

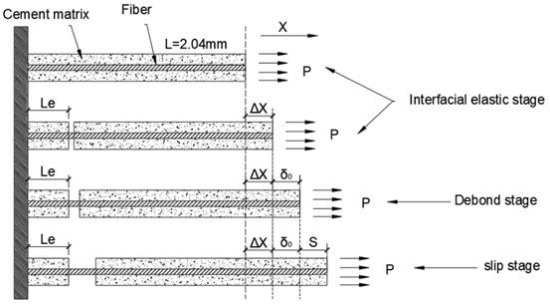

Fig. 5 Fiber-matrix joint constitutive relation model analysis unit

In the elastic stage of the interface, as the deformation of the cementitious matrix is neglected, the displacement of the fiber and matrix composite can be considered negligible prior to matrix cracking. Following matrix cracking, the relative displacement X generated within this composite originates primarily from the elastic deformation of the fiber-matrix interface on both sides of the crack. Therefore, the displacement ΔX at the matrix surface during the elastic interfacial stage can be determined from Equation (6).

$$\Delta x = \frac{4P_{d0}L_f}{\pi E_I d_f^2} \quad (6)$$

Where P_{d0} represents the initial load value of the fiber at the debonding stage, E_I represents the elastic modulus of the fiber, L_f represents the fiber length, and d_f represents the fiber diameter.

When the load reaches the initial value of P_{d0} in the deboned stage, the plant fiber starts to debone from the cement matrix, L_e is determined by the position where the fiber cracks. During the deboned stage Δx are negligible. Therefore, the displacement chosen is still δ_0. During the slip stage of fibers, the fiber is treated as a rigid body, with only its translational displacement S being considered.

The depth at which the fiber is buried is an important factor in determining the load-displacement curve of a single fiber pull-out. Different burial depths result in different load-displacement curves for the fibers. Equation (3) indicates that the burial depth primarily affects complete debonding pull-out distance of fiber δ_0 and does not influence the changing trend during the debonding stage. However, the burial depth significantly impacts the slip stage of fiber. Therefore, a two-dimensional single-fiber pull-out simulation is carried out for fibers with different burial depths.

Verification of the PFRCC panel model

The three-point bending simulation of the PFRCC panel is conducted to validate the numerical model's accuracy, and the results are compared with test data.

Through the Coupling command, the force surface of the rigid loading end was coupled to the reference point. All degrees of freedom were constrained except for the translational degree of freedom in the Y direction. The finite element model adopted the displacement loading method, and the negative displacement along the Y direction was applied to the reference point. Rigid bearings were set at both ends of the specimen, and boundary conditions were imposed at the bottom of the rigid body to completely fix the constraint to simulate the actual support, which was consistent with the test.

2.4 Case study on the application of PFRCC permanent formwork in foundation beams

Project summary

This case study was conducted on a community construction project in Lanzhou City, Gansu Province. The subject was a foundation beam with a rectangular cross-section, measuring 700 mm in height and 300 mm in width. According to the size of the foundation beam, the side formwork was assembled by PFRCC panels with a size of 1000 mm (length) × 700 mm (width) × 18 mm (thickness), and the beam fixture was set every 1000 mm. The bottom formwork was assembled by PFRCC panels with a size of 1000 mm (length) × 300 mm (width) × 18 mm (thickness). According to the three-point bending test, the bending design strength of the PFRCC panel is f_d =13.7×106 N/m². The construction process and field test of the PFRCC foundation beam permanent formwork are shown in Figures 6 and 7.

Fig. 6 PFRCC foundation beam permanent formwork picture

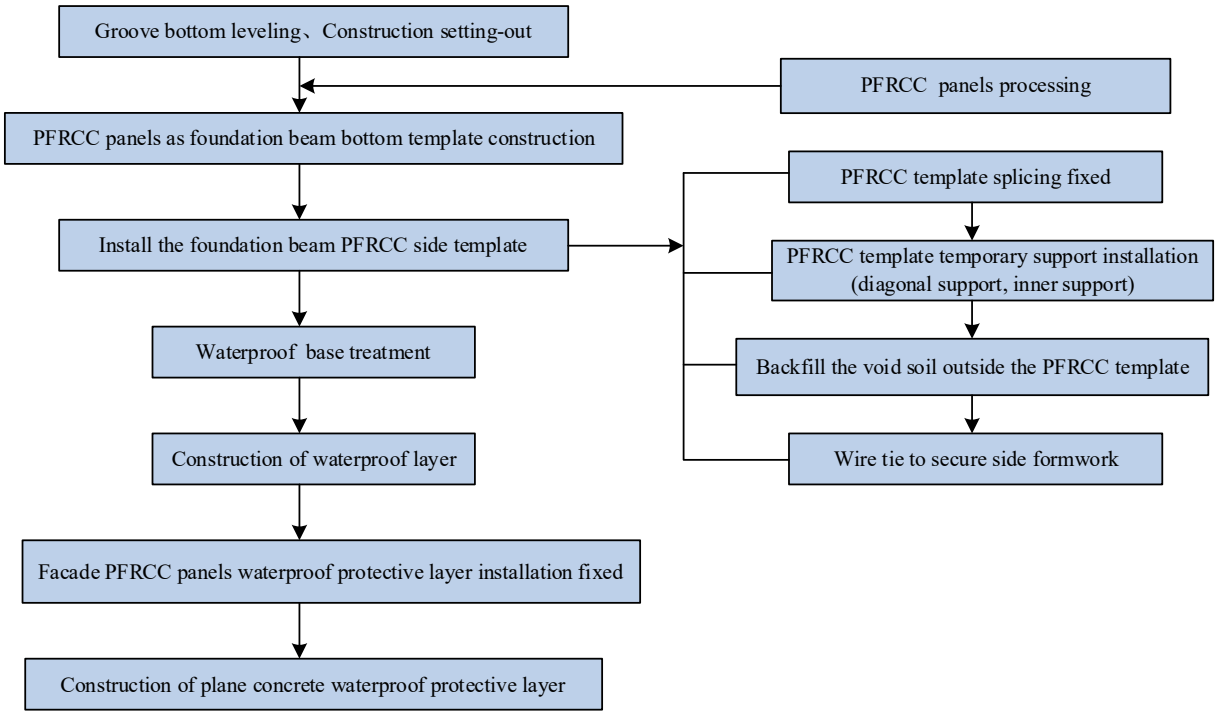

Fig. 7 Process flow chart of PFRCC foundation beam formwork

PFRCC foundation beam permanent formwork load calculation

In Figure. 8, according to the design and field test analysis of the PFRCC foundation beam formwork, the primary loads of the side formwork are the lateral pressure of the newly poured concrete and the soil pressure generated by the backfill. The main loads of the bottom formwork are the weight of the newly poured concrete and the weight of the steel bar. The specific loads are shown in Table 4 and Table 5.

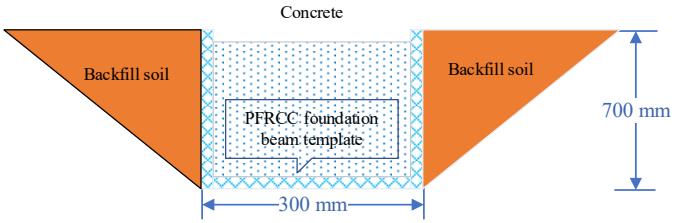

Fig. 8 Schematic diagram of foundation beam formwork model

Table 4. Bottom formwork load

Load project	The standard value of load (N/m²)	Load partial coefficient	Design load value (N/m²)
New pouring concrete weight	16800	1.35	22680
Self-weight of steel bars	1500	1.35	2025

Table 5. Side formwork load

Load project	The standard value of load (N/m²)	Load partial coefficient	Design load value (N/m²)
New pouring concrete weight	16800	1.35	22680
Backfill soil pressure	14000	1.35	18900

Finite element analysis of the PFRCC foundation beam permanent formwork

The finite element analysis of the permanent formwork of the PFRCC foundation beam was carried out using the separated element model. The plant fiber-reinforced cementitious composites panel was divided into units to calculate the stress of the whole model. The side formwork adopts PFRCC panels of 1000 mm (length) × 700 mm (width) × 18 mm (thickness) for assembly, and a beam fixture was set every 1000mm. The bottom formwork adopts PFRCC panels with a size of 1000 mm (length) × 300 mm (width) × 18 mm (thickness) for assembly and splicing.

Simulation of boundary conditions is an essential step in finite element analysis. As shown in Figure. 9, the constraints on the side formwork of the model were the support constraints of the external support of the whole formwork to the formwork, in which the beam fixture was completely fixed, and the part of the bottom formwork contacting the foundation soil was also wholly fixed.

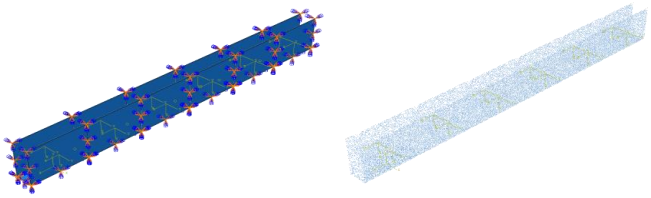

(a)Permanent formwork model (b)Fiber model of the formwork

Fig. 9 Permanent formwork model of the foundation beam

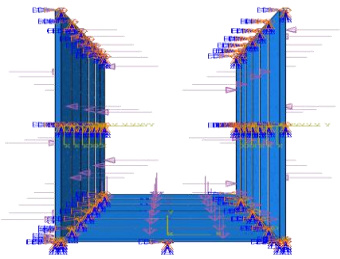

Fig. 10 Permanent formwork load cross-section of the foundation beam

As shown in Figure. 10, In the analysis of composite structures, finite element models typically fall into three categories: discrete, combined, and integrated models. For this study on the PFRCC foundation beam permanent formwork test, we utilize a discrete element model based on the specimen's configuration and the actual loading conditions. In this model, the components of the PFRCC, including the cement matrix and the fiber elements, are treated as separate entities to determine the overall distribution of stress. The specimen is represented as a solid body, while the various loads acting on it—such as the lateral pressure from the freshly poured concrete on the inner side of the formwork, the earth pressure from the backfill soil on the outer side, and the self-weight of the reinforced concrete pressing down on the bottom of the formwork are converted into uniformly distributed loads applied to the formwork.

3. Results and Discussion

3.1 Three-point bending test results of PFRCC panel

It can be seen from Table 6 and Figure. 11 that the failure load (Pm) of specimen I is 1468.8 N, the corresponding peak displacement (δ_m) is 1.05 mm, and the bending strength (σ_m) is 13.6 MPa. The failure load (Pm) of specimen II is 1488.9 N, the corresponding peak displacement (δ_m) is 1.18 mm, and the bending strength (σ_m) is 13.8 MPa. The failure load (Pm) of specimen III is 1483.3 N, the corresponding peak displacement (δ_m) is 1.23 mm, and the bending strength (σ_m) is 13.7 MPa.

It can be obtained that the mean value of the failure load (Pm) of this type of PFRCC panel is 1480.3 N, the mean value of the corresponding peak displacement (δ_m) is 1.15 mm, and the bending strength (σ_m) is 13.7 MPa.

Table 6. Three-point bending strength test results of PFRCC panels

Specimen number	P_m (N)	δ_m (mm)	σ_m (MPa)
Specimen I	1468.8	1.05	13.6
Specimen II	1488.9	1.18	13.8
Specimen III	1483.3	1.23	13.7

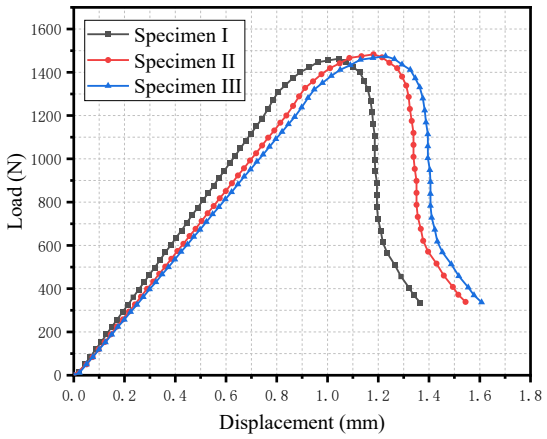

Fig. 11 Load-displacement curve of three-point bending test

3.2 Effect of burial depths on load-displacement curves of fiber single fiber pull-out

In Figure. 12, it can be seen that the bond-slip constitutive of plant fiber with 0.6 mm burial depth is closer to the average constitutive. Therefore, this paper uses the fiber-matrix joint constitutive relation model with 0.6 mm burial depth as shown in Figure. 13.

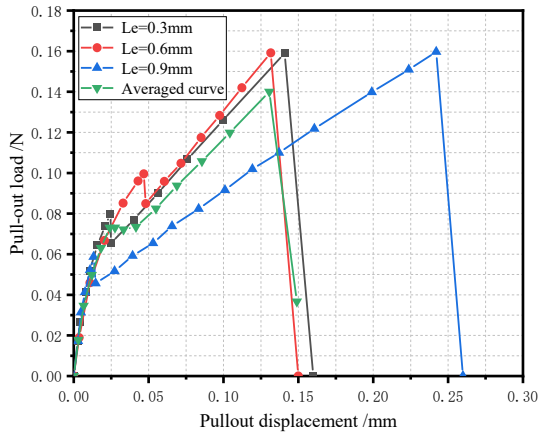

Fig. 12 Load-displacement curves of fiber single fiber pull-out with different burial depths

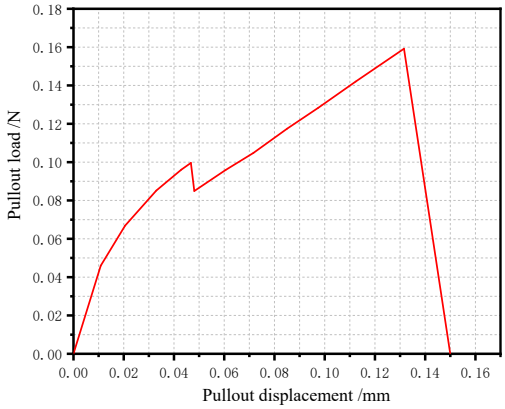

Fig. 13 Fiber-matrix joint constitutive load-displacement curve

In finite element software, stress and strain values are required when the fiber-matrix joint constitutive relation model is input. In this regard, the ordinate is divided by the fiber cross-sectional area, and the abscissa is divided by the fiber length to obtain the stress and strain respectively. The resulting Fiber-matrix joint constitutive relation model is shown in Figure. 14. When the strain is between 0 and 0.00539, the interface is in the elastic stage. At this point, the plant fibers bond well with the matrix, and the shear stress gradually increases, reaching its maximum at the fiber pullout point. As the strain increases from 0.00539 to 0.022, the interface enters the debonding stage. During this stage, the fibers begin to be deboned from the pullout point; the deboned section maintains a constant maximum shear stress while the stress in the bonded section progressively increases. The debonding process concludes when it propagates from the pullout segment to the embedded end of the fiber. When the strain ranges from 0.024 to 0.065, the interface is in the slip hardening stage. Here, the shear stress distributes uniformly along the fiber surface, and fiber behavior is primarily governed by sliding friction. Additionally, Figure 14 clearly shows that during the strain interval of 0.022 to 0.024, the entire fiber transitions from debonding to slipping. At this point, the dominance shifts from chemical bonding to frictional control, resulting in a stress release process that is accompanied by a sudden drop in external load. Following this, the fibers enter the slip hardening stage. Due to significant surface abrasion of the plant fibers during pullout, the friction coefficient progressively increases, leading to the slip hardening phenomenon, characterized by a gradual increase in sliding friction. When the strain ranges from 0.065 to 0.074, fiber fracture occurs, reducing the fiber stress value to zero. Consequently, the fibers cease to provide a bridging effect against matrix cracking. To simulate the sudden stress, drop after fiber pullout failure, a point representing abrupt stress reduction is added at the tail end of the model curve, with the strain approaching the actual pullout failure strain to indicate fiber failure.

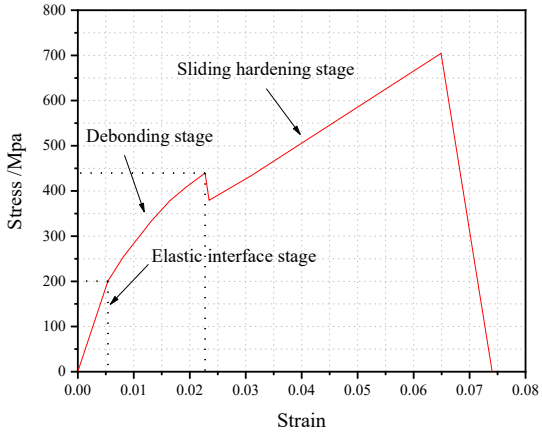

Fig. 14 Fiber-matrix joint constitutive stress-strain curve

3.3 Three-point bending numerical simulation results of PFRCC panel

It can be seen from Figure. 15 and Figure. 16 that the numerical simulation failure load of the PFRCC panel with cement of compressive strength of 45.6 MPa as the matrix, the plant fiber content of about 6 %, and thickness of 18 mm is 1575.7 N, the corresponding peak displacement is 1.16 mm, and the bending strength is 14.59 Mpa. The numerical model of the PFRCC panel established in this paper can fit the experimental data well, proving the numerical model's correctness and providing a reliable basis for the finite element simulation of the PFRCC panels for foundation beam formwork.

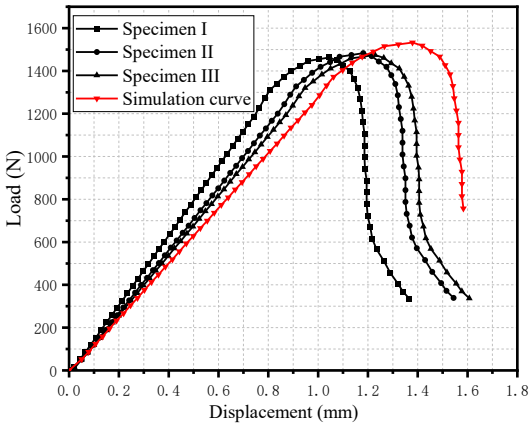

Fig. 15 Simulated bending load-displacement curve of PFRCC panel

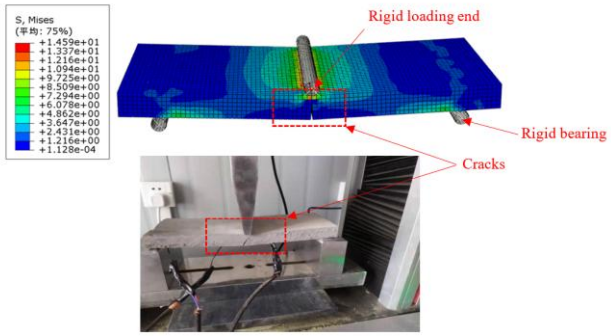

Fig. 16 Stress cloud diagram of PFRCC panel three-point bending specimen failure

3.4 Bending stress of PFRCC foundation beam permanent formwork

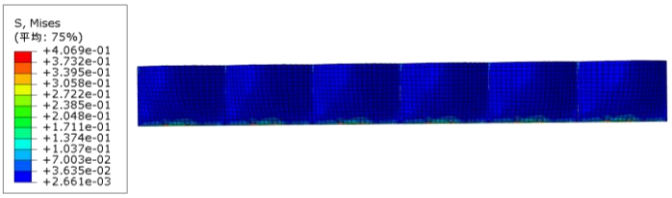

(a)PFRCC side formwork cement matrix stress

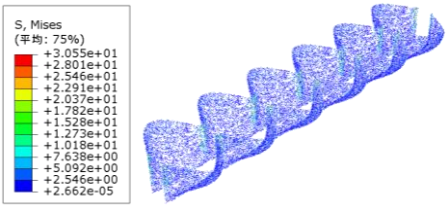

(b)PFRCC side formwork fiber stress

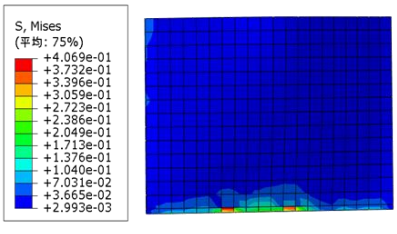

(c)Unit PFRCC side formwork cement matrix stress

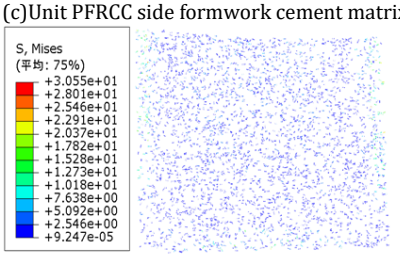

(d)Unit PFRCC side formwork fibers stress

Fig. 17 PFRCC side formwork stress nephogram (MPa)

The bending design strength of the PFRCC panels used in this research, evaluated through the three-point bending test, is identified as f_d = 13.7 × 106 N/m^2. In Figure. 17, the maximum bending stress of the cement matrix part of the 18 mm thick PFRCC foundation beam side formwork is located at the splicing of the side formwork and the bottom formwork, and the maximum bending stress is SMN = 0.4069 MPa < 13.7 MPa, which satisfies the bending strength condition. The incorporation of plant fibers into the cement matrix panel significantly enhances its load-bearing capacity, as evidenced by the maximum bending stress of *SMN* = 30.55 MPa observed in the fiber-reinforced section. This improved mechanical performance demonstrates the composite material's effectiveness in withstanding lateral formwork pressure.

In Figure. 18, the maximum bending stress of the cement matrix part of the 18 mm thick PFRCC foundation beam bottom formwork is located in the middle of the bottom formwork, and the maximum bending stress is *SMN* = 0.187 MPa < 13.7 MPa, which satisfies the bending strength condition. The maximum bending stress of the fiber part is *SMN* = 5.728 MPa.

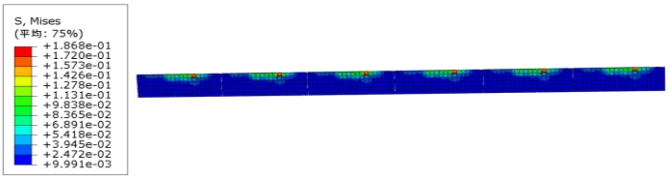

(a)PFRCC bottom formwork cement matrix stress

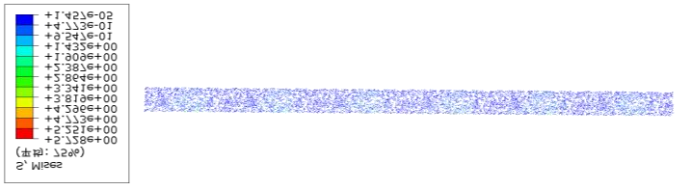

(b)PFRCC bottom formwork fibers stress

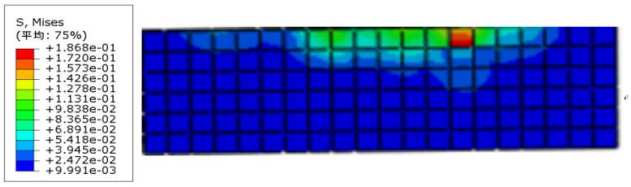

(c) Unit PFRCC bottom formwork cement matrix stress

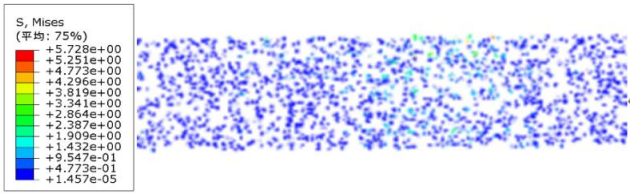

(d) Unit PFRCC bottom formwork fibers stress

Fig. 18 PFRCC bottom formwork stress nephogram (MPa)

To sum up, the bending stress of an 18 mm thick PFRCC panel as a permanent foundation beam formwork meets the requirements. And the addition of plant fibers to the cement matrix can effectively bear the pressure of the formwork.

3.5 Bending deformation of PFRCC foundation beam permanent formwork

According to the Code for construction of concrete structures (Ministry of Housing and Urban-Rural Development of the People's Republic of China, 2012), the deformation limits for formwork and supports shall comply with the provisions of Table 7:

Table 7. List of allowable values of deflection

The project name	Allowable deflection
Structure surface exposed formwork and back ridge	*L* / 400
Structure surface hidden formwork and back ridge	*L* / 250
Compression deformation or elastic deflection of the bracket	*L* / 1000

Where L represents the calculation span of the bending member.

In Figure. 19, the maximum deformation of the side formwork of the 18 mm thick PFRCC foundation beam is located in the middle of the span. The deformation of the cement matrix and the deformation of the fiber are the same. The maximum deformation is DMX = 1.528 mm < L/400=2.5 mm, which satisfies the stiffness condition.

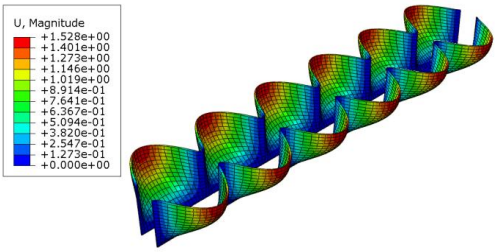

(a)PFRCC side formwork cement matrix deformation

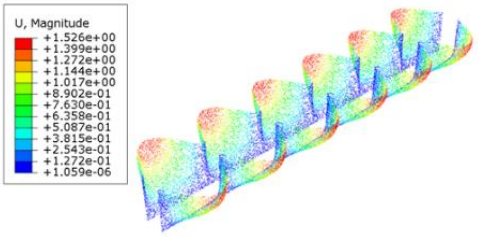

(b)PFRCC side formwork fibers deformation

Fig. 19 PFRCC side formwork deformation nephogram (mm)

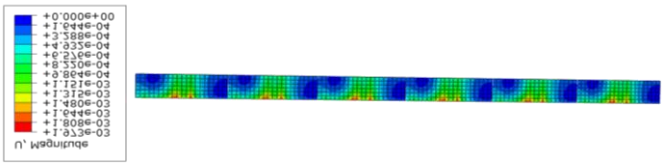

(a)PFRCC bottom formwork cement matrix deformation

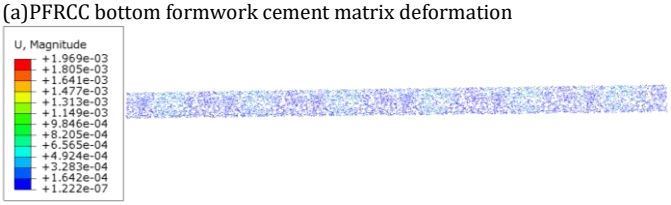

(b)PFRCC bottom formwork fibers deformation

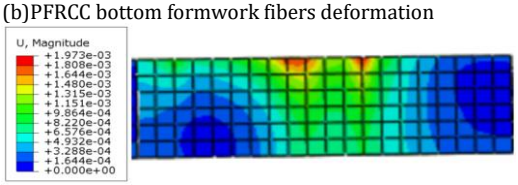

(c)Unit PFRCC bottom formwork cement matrix deformation

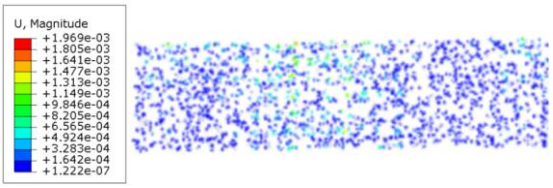

(d) Unit PFRCC bottom formwork fibers deformation

Fig. 20 PFRCC bottom formwork deformation nephogram (mm)

In Figure. 20, the maximum deformation of the 18mm thick PFRCC foundation beam bottom formwork is located at the mid-span, the maximum deformation of the cement matrix part and the fiber part is DMX = 1.502 mm < L/400 = 2.5 mm, which satisfies the stiffness condition.

In summary, the maximum bending deformation of the 18mm thick PFRCC foundation beam integral formwork is located at the mid-span of the side formwork, and the maximum deformation is DMX = 0.002268 mm < L/400=2.5 mm, which satisfies the stiffness condition. So, 18 mm thick PFRCC panels meet the foundation beam permanent formwork requirements.

4. Conclusion

This paper examines the feasibility of using PFRCC panels as permanent formwork to replace traditional brick formwork for foundation beams. The study is based on a practical engineering project in Lanzhou City. The analysis used a combination of field tests and numerical simulations, resulting in the development of a comprehensive, rapid, and efficient construction solution. The main conclusions are as follows:

1) The numerical simulation based on the proposed fiber–matrix joint constitutive model yields failure load, peak displacement, and bending strength values that are in close agreement with the experimental means. The deviations between simulated and experimental results are approximately 6.4% for failure load, 0.9% for peak displacement, and 6.5% for bending strength. These minor discrepancies can be

attributed to the idealized boundary conditions and material homogeneity assumptions inherent in the numerical model. Moreover, the close agreement of the simulated and experimental load–displacement curves further validate the reliability and accuracy of the finite element model for PFRCC formwork.

2) In conclusion, the PFRCC panels proved to be an effective permanent formwork solution, with a maximum bending stress of 0.4 MPa, well below the allowable limit of 13.7 MPa. This stress occurs at the joint between the side and bottom formwork, confirming that the bending strength satisfies the required conditions.
3) The PFRCC panels also function effectively as permanent formwork for foundation beams, with consistent deformation observed in both the cement matrix and fibers. The maximum deformation of 1.5 mm occurs at the midpoint of the side formwork, which is less than L/400 = 2.5 mm. This indicates that stiffness and deformation performance meet the design requirements.
4) Based on this research, PFRCC panels with a thickness of 18 mm can be applied as permanent formwork for foundation beams. Future work will focus on improving the fiber–matrix constitutive model, for example, by incorporating hook-shaped plant fibers to enhance joint performance.

Acknowledgments

This research is supported in part by the National Natural Science Foundation of China (Grant no. 52178389).

Conflicts of Interest

The authors hereby confirm the absence of any financial, personal, or professional conflicts of interest that could be perceived as influencing the research findings or the publication of this work.

References

Arslan, M., Şimşek, O., Subaşı, S. (2005). Effects of formwork surface materials on concrete lateral pressure. Construction and building materials, 19(4), 319-325. DOI: https://doi.org/10.1016/j.conbuildmat.2004.07.007

Conforti, A., Zerbino, R., Plizzari, G. A. (2019). Influence of steel, glass and polymer fibers on the cracking behavior of reinforced concrete beams under flexure. Structural Concrete, 20(1), 133-143. DOI: https://doi.org/10.1002/ suco. 201800079

Empelmann, M., Oettel, V., Cramer, J. (2020). Berechnung der Rissbreite von mit Stahlfasern und Betonstahl bewehrten Betonbauteilen. Beton-und Stahlbetonbau, 115(2), 136-145. DOI: https://i.org/10.1002/ best. 2019000 65

Geng, J., Cheng, W., & Liu, G. (2024). Enhancing interface shear performance and bending resistance of UHPC permanent formwork for composite short beams by different interface treatment. Journal of Building Engineering, 85, 108736. DOI: https://doi.org/10.1016/j.jobe.2024.108736

Guo, Y. H., Li, L., Yang, C. X., Shi, Y. Q. (2022). Research progress of plant fiber reinforced concrete. Bulletin of the Chinese Ceramic Society, 41(10), 3347-3358.

Haido, J. H. (2020). Flexural behavior of basalt fiber reinforced concrete beams: Finite element simulation with new constitutive relationships. Structures, 27, 1876-1889. DOI: https://doi.org/10.1016/j.istruc.2020.08.005

Hemmatian, A., Jalali, M., Naderpour, H., & Nehdi, M. L. (2023). Machine learning prediction of fiber pull-out and bond-slip in fiber-reinforced cementitious composites. Journal of Building Engineering, 63, 105474. DOI: https://doi.org/10.1016/j.jobe.2022.105474

Huang, B. T., Li, Q. H., Xu, S. L., Li, C. F. (2017). Development of reinforced ultra-high toughness cementitious composite permanent formwork: experimental study and digital image correlation analysis. Composite Structures, 180, 892-903. DOI: https://doi.org/10.1016/j.compstruct.2017.08.016

Hall, J. E., Mottram, J. T. (1998). Combined FRP reinforcement and permanent formwork for concrete members. Journal of Composites for Construction, 2(2), 78-86. DOI: https://doi.org/10.1061/(ASCE)1090-0268(1998)2:2(78)

Keskisaari, A., Butylina, S., Kärki, T. (2016). Use of construction and demolition wastes as mineral fillers in hybrid wood-polymer composites. Journal of Applied Polymer Science, 133(19). DOI: https://doi.org/10.1002/app.43412

Kochova, K., Gauvin, F., Schollbach, K., & Brouwers, H. J. H. (2020). Using alternative waste coir fibres as a reinforcement in cement-fibre composites. Construction and Building Materials, 231, 117121. DOI: https://doi.org/10.1016/j.conbuildmat.2019.117121

Kim, G. B., Pilakoutas, K., Waldron, P. (2008). Development of thin FRP reinforced GFRC permanent formwork systems. Construction and building materials, 22(11), 2250-2259. DOI: https://doi.org/10.1016/j.conbuildmat.2007.07.029

Li, V. C. (1993). From micromechanics to structural engineering the design of cementitious composites for civil engineering applications. Doboku Gakkai Ronbunshu, 10(2), 37-48. https://doi.org/10.2208/jscej.1993.471_1

Leblouba, M., Altoubat, S., Karzad, A. S., Maalej, M., Barakat, S., & Metawa, A. (2022). Impact response and endurance of unreinforced masonry walls strengthened with cement-based composites. Structures, 36, 262-279. DOI: https://doi.org/10.1016/j.istruc.2021.12.028

Li, Q. H, Gao, X., Xu, S. L., Zhao, X. (2015). Permanent formwork of ultra-high toughness cementitious composites added with nano-SiO2. China civil engineering journal, 48(06), 9-16.

Li, M., Khelifa, M., Khennane, A., El Ganaoui, M. (2019). Structural response of cement-bonded wood composite panels as permanent formwork. Composite Structures, 209, 13-22. DOI: https://doi.org/10.1016/j.compstruct.2018.10.079

Li, W., Wang, Z., Li, L., Du, T., & Sun, L. (2023). Experimental study on axial compression of hybrid fiber cement-based composite column with circular cross section. Structures, 53, 664-676. DOI: https://doi.org/10.1016/j.istruc.2023.04.061

Ministry of Housing and Urban-Rural Development of the People's Republic of China. (2012). Code for construction of concrete structures (GB 506666-2011). China Architecture & Building Press, Beijing.

Meng, W., Khayat, K. H. (2016). Experimental and numerical studies on flexural behavior of ultrahigh-performance concrete panels reinforced with embedded glass fiber-reinforced polymer grids. Transportation Research Record, 2592(1), 38-44. DOI: https://doi.org/10.1016/j.conbuildmat.2017.02. 002 https://doi.org/10.3141/2592-05

Oettel, V. (2023). Steel fiber reinforced RC beams in pure torsion-Load-bearing behavior and modified space truss model. Structural Concrete, 24(1), 1348-1363. DOI: https://doi.org/10.1002/suco.202200031

Oettel, V., Schulz, M., Haist, M. (2022). Empirical approach for the residual flexural tensile strength of steel fiber-reinforced concrete based on notched three-point bending tests. Structural Concrete, 23(2), 993-1004. DOI: https://doi.org/10.1002/suco.202100565

Prosk, T., Khayat, K. H., Omran, A., Leitzbach, O. (2014). From pressure generated by fresh concrete: a review about practice in formwork design. Materials and structures, 47(7), 1099-1113. https://doi.org/10.1617/s11527-014-0274-y

Puente, I., Santilli, A., Lopez, A. (2010). Lateral pressure over formwork on large dimension concrete blocks. Engineering Structures, 32(1), 195-206. DOI: https://doi.org/10.1016/j.engstruct.2009.09.006

Standardization Administration of China. (2014). Test methods for fiber cement products (GB/T 7019-2014). Standards Press of China, Beijing.

Tiberti, G., Germano, F., Mudadu, A., Plizzari, G. A. (2018). An overview of the flexural post-cracking behavior of steel fiber reinforced concrete. Structural Concrete 19(3), 695-718. DOI: https://doi.org/10.1002/suco.201700068

Turku, I., Keskisaari, A., Kärki, T., Puurtinen, A., Marttila, P. (2017). Characterization of wood plastic composites manufactured from recycled plastic blends. Composite Structures, 161, 469-476. DOI: https://doi.org/10.1016/j.compstruct.2016.11.073

Tian, H., Zhou, Z., Zhang, Y., & Wei, Y. (2020). Axial behavior of reinforced concrete columns with ultra-high performance concrete stay-in-place formwork. Engineering Structures, 210, 110403. DOI: https://doi.org/10.1016/j.engstruct.2020.110403

Väntsi, O., Kärki, T. (2014). Utilization of recycled mineral wool as filler in wood-polypropylene composites. Construction and Building Materials, 55, 220-226. DOI: https://doi.org/10.1016/j.conbuildmat.2014.01.050

Wang, X., Liu, H., Ju, Y., & Wang, D. (2021). Experimental and analytical models of flexural behavior of U-shaped reactive powder concrete permanent beam formworks. Construction and Building Materials, 300, 123670. DOI: https://doi.org/10.1016/j.conbuildmat.2021.123670

Wang, L. H., Shi, W. H., Qian, L. P., Bai, Y. L., Liu, S. Z., & Yang, Z. Q. (2025). Flexural behaviors of GFRP-reinforced Engineered Cementitious Composite (ECC)-concrete composite beams. Engineering Structures, 332, 120097. DOI: https://doi.org/10.1016/j.engstruct.2025.120097

Zhang, W., Huang, J., Li, Z., Huang, C. (2016). An experimental study on the lateral pressure of fresh concrete in formwork. Construction and building materials, 111, 450-460. DOI: https://doi.org/10.1016/j.conbuildmat.2016.02.067

Disclaimer